

ADAPTIVE POWER- SHARING STRATEGY IN HYBRID AC/DC MICRO GRID FOR ENHANCING VOLTAGE AND FREQUENCY REGULATION BY HYBRID FOPID CONTROLLER

¹M.Mary Linda, Professor in Department of EEE,
²S.Sarathkumar, PG Student in Department of EEE,
KIT-Kalaignarkarananithi Institute of Technology, Coimbatore, Tamilnadu

Abstract - In this article, a fractional-order proportional integral- differential (FOPID) controller and its modified structure, called a Hybrid FOPID controller, are presented. To guarantee optimal system performance, the gains of the proposed Hybrid FOPID controllers are well-tuned. The proposed controllers are assessed in a hybrid system with two domains, where each domain contains a DC Grid and AC grid. This paper introduces a new adaptive control strategy for power-sharing in a hybrid AC/DC Microgrid (HMG). The existing interlink converter (ILC) control methods exhibit limitations under heavy load and contingency conditions. To overcome this limitation, a bidirectional control strategy is proposed for the ILC, which effectively coordinates battery energy storage systems (BESSs) in both sub-grids while justifying stress on the ILC and BESSs. The control strategy utilizes the state of charge (SoC) and instantaneous power of the BESSs to stabilize frequency and DC voltage on the AC and DC sub-grids, respectively, enabling autonomous operation and plug-and-play capability. Stability analysis employing root locus and a stress level relaxation index for BESSs are presented. Performance evaluation based on the moving mean square error criterion validates the effectiveness of the control strategy. Simulation results using MATLAB/SIMULINK demonstrate the superior performance of the proposed strategy in regulating both voltage and frequency within the system over the existing control approaches. Furthermore, the proposed approach significantly reduces stress levels on the BESSs in different operation conditions.

1. INTRODUCTION

A microgrid is a small-scale network comprising controllable distributed generation units, loads, and battery energy storage systems (BESSs) that can operate in grid-connected or islanded mode [1]. A hybrid microgrid (HMG) includes AC and DC microgrids with loads and one or more interlinking devices as a tie between subsystems [2].

HMGs bring excellent advantages from both the grid perspective and the customers' point of view. A HMG eliminates several successive power converters to convert the AC power to DC and vice versa, reducing overall system costs and losses. In addition, by reducing the required number of power converters, the reliability and efficiency of the microgrid will be boosted because the number of switches is reduced [3-5]. However, choosing a suitable approach for interlinking and adopting the most effective and efficient power-sharing between sub-grids and each unit is challenging. An inappropriate strategy may increase the stress level on the interlink converter, leading to HMG instability and resulting in a complete network outage [6,7]. Bidirectional converters, commonly called interlink converters (ILCs), are used to couple the AC and DC sub-grids, seamlessly exchanging the power between the two subsystems with the aim of voltage and frequency regulation [8].

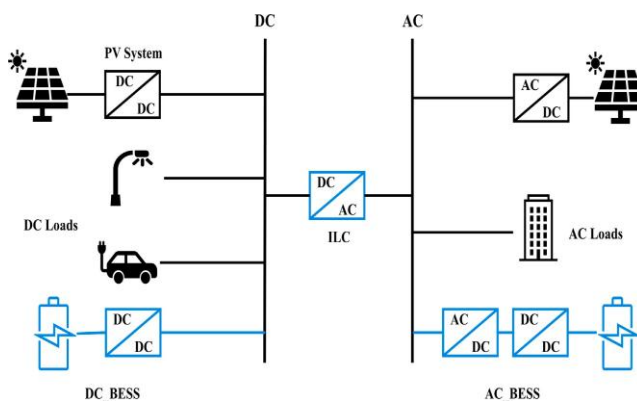


Fig 1.1 AC/DC Microgrids

In both AC and DC sub-grids, the power or load should be shared proportionally among generation units according to their nominal capacities in an effective manner. In AC microgrids (ACMGs), active and reactive power-sharing should be associated with frequency and voltage regulation [9,10]. The voltage stability in DC microgrids (DCMGs) is achieved through effective real power sharing [11,12]. In [13], a finite-state-machine-based controller was proposed instead of the conventional inner controller layer of the DC micro grid with a faster response. The plug-and play reflects the capability of the micro grid to regulate its voltage and frequency under different operating conditions, such as generation units disconnections/connections and load changes [14]. The droop control method with plug-and-play capability has been vastly used for load-sharing in ACMGs and DCMGs [15–17]. The ILC links AC and DC sub-grids to maintain the power balance. To achieve this goal, the voltage at the DC terminal and frequency at the AC terminal of the ILC are utilized to compare the status of the sub-grids, which is then used to implement a power-sharing strategy between them [18,19]. Different strategies and devices for interfacing the ACMG and the DCMG were discussed in [20], and it was concluded that using a single ILC may outweigh the other methods in terms of economic consideration, reliability improvement, and feasibility.

DC voltage to compare the ACMG and DCMG statuses and control the power-sharing between them [21]. However, this strategy has some drawbacks, such as a complex control strategy, challenges in voltage regulation and power quality issues [22]. In [23–25], the authors proposed a global power-sharing approach by distributing the loads equally between AC and DC subgrids even though their generation capacities were different. This approach increases pressure on the ILC as it is not a capacity-oriented power-sharing strategy. Also, a fault in each sub-grid may lead to the instability in the whole system. A master-slave control method for load-sharing and harmonic mitigation was proposed in [26], which requires high bandwidth communication for data acquisition and the exchange information between parallel ILCs. Authors in [27] considered both AC and DC side voltages as the decision parameters for power exchange. Furthermore, a line impedance estimation technique was used to realize the dynamic condition of the network. However, the ILC had unidirectional power exchangeability. Therefore, optimal power-sharing was not achievable. Common bus technique was proposed in [28]. In this technique, each generation source tries to regulate the voltage at the point of common coupling (PCC) bus rather than its local bus voltage, employing a decentralized approach through the utilization of the droop control method. While this approach improved voltage regulation under normal load conditions, its performance under heavy load conditions is unsatisfactory. In [29], capacity-based power-sharing in a HMG was investigated, but the control strategy was not adaptive as it was only working based on the AC frequency and DC voltage. In other words, the performance of the control system was not evaluated in contingency and heavy load conditions. Similarly, the authors in [30] proposed a master-slave control strategy where the accuracy of power sharing has been improved, especially when a communication failure occurs, by introducing a coordination factor into the system. However, the loads were not shared based on each subsystem generation capacity. A central energy storage system was utilized in [31] to support both AC and DC subsystems. However, the voltage and frequency regulation control strategy resulted in high over-shoots or undershoots. A global power-sharing strategy was proposed in [32] which adopts a superimposed AC voltage onto the nominal voltage of the DC sub-grid, despite the nominal capacities of the AC and DC microgrids being different, which may increase the stress level on the ILC. A unidirectional, centralized secondary control layer for reducing the error of voltage and frequency regulation was proposed in [33]. However, the control system was only designed to transfer power from the DC subsystem to the AC side to compensate for the power deficit in the AC microgrids. A cost-based, multi-mode power-sharing strategy was proposed in [34]. However, its performance was not evaluated under heavy load conditions when the control strategy is required to make a decision based on system regulation or cost. Similarly, an efficiency-improved and cost-effective approach for power-sharing in normal load conditions was considered in [35]. An adaptive control of the ILC based on the continuous mixed Pnorm algorithm was proposed in [36]. However, the performance of the adaptive control in overload conditions to regulate the voltage and frequency is not satisfactory. A nonlinear exponential droop control strategy for controlling power-sharing between AC and DC subsystems was proposed in [37]. The mathematical expressions of this method are

discussed in Appendix. While this method enhanced the accuracy of power sharing and improved voltage and frequency stability within the system, its performance in regulating voltage and frequency under heavy load conditions is not desirable.

Although optimal capacity-oriented power-sharing was discussed in the literature, there is a need for further attention on adaptive power-sharing strategies that can increase system stability during heavy load conditions and reduce stress on the ILC. This paper proposes and investigates a new autonomous adaptive control strategy that considers the state of charge (SoC) level of the BESS and the amount of power available for power sharing. This strategy aims to improve HMG stability and enhance frequency and voltage regulation. The contributions of this research can be summarized as follows:

- (A) Supporting the sub-grids of the HMG in high load and medium load conditions by importing power from the other side in an adaptive manner by considering the characteristics of batteries, including instantaneous power and SOC level to mitigate the stress on the BESS and reduce the likelihood of losing system stability.
- (B) Enhancing voltage and frequency regulation of the HMG in high load conditions by adopting the proposed adaptive control loop.
- (C) Proposing an index for evaluating the stress level on BESS based on its SoC and instantaneous discharge power.

The rest of this paper is structured as follows. In Section 2, the proposed adaptive control strategy is presented. Section 3 investigates the stability of the proposed control system.

1. Proposed adaptive control strategy

The topology of the proposed control strategy is depicted in Fig. 2.1. This proposed control architecture works based on the SoC level and instantaneous power of the sub-grid's BESS. The proposed adaptive control strategy is autonomous. In other words, it operates based on the status of the BESSs of the subsystems without any concern about the type and number of the generation sources and loads, as long as the planning and design criteria of the HMG have been met. The concept of the suggested control system is illustrated in Fig. 2.2.

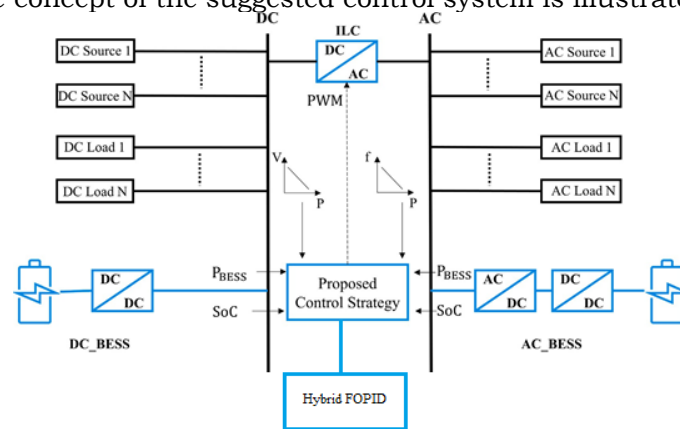


Fig. 2.1 The proposed control system topology.

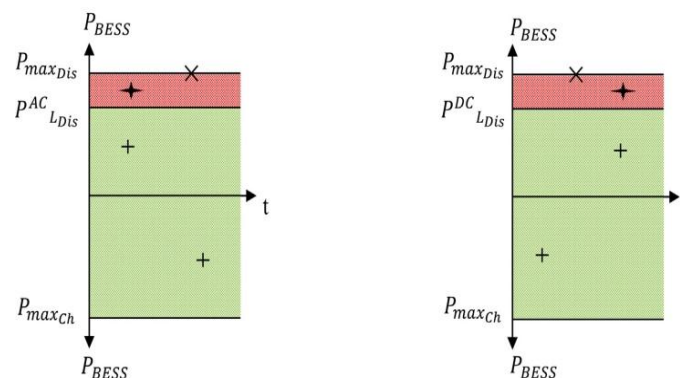


Fig. 2.2 Conceptual illustration of the proposed control strategy.

Based on Fig. 2, six general operation scenarios may happen:

1. Green-Green Operation Regions:

When both BESSs operate in the green region it is interpreted that both ACMG and DCMG are in a light load condition, and each BESS can be in charge mode or discharge mode. As a result, there is no need to exchange power between them, and therefore, the ILC works at the minimum exchange power rate condition. However, due to the interconnected nature of the ACMG and DCMG, there may still be a slight power exchange between them, although it is considered insignificant. This minimal power exchange rate can be regarded as the minimum value of power transfer between the two sub-grids. Also, the stress level on the ILC is at the minimum. The mathematical expression of this scenario is as below:

$$\begin{cases} P_{BESS}^{AC}(t) \leq P_{LDis}^{AC} \\ P_{BESS}^{DC}(t) \leq P_{LDis}^{DC} \end{cases} \quad (1)$$

2. Green-Red Operation Regions:

In this scenario, one of the BESSs works in the green area, while the other operates in the red region. This condition indicates that one of the microgrids is working in a light load condition. In contrast, another sub-grid is in a high load condition, so the ILC should transfer power from the microgrid with surplus power to the MG in the red zone to reduce the stress level on the BESS operating in the red region. This scenario can be expressed as:

$$\begin{cases} P_{BESS}^{AC}(t) \leq P_{LDis}^{AC} \\ P_{BESS}^{DC}(t) > P_{LDis}^{DC} \end{cases} \quad \text{or} \quad \begin{cases} P_{BESS}^{AC}(t) > P_{LDis}^{AC} \\ P_{BESS}^{DC}(t) \leq P_{LDis}^{DC} \end{cases} \quad (2)$$

3. Green Region-Maximum Discharge Rate:

This scenario is one of the critical situations for the HMG. One of the BESSs operates in the green region while the other BESS is discharging with its maximum rating power. In this condition, according to the proposed adaptive control strategy, the ILC plays a considerable role in maintaining the system in its stable operation boundaries. The sub-grid with the battery operating in the red zone imports power to alleviate the pressure on its BESS. Otherwise, by continuously discharging the battery, the microgrid moves towards collapse. The mathematical expression of this scenario is as follows:

$$\begin{cases} P_{BESS}^{AC}(t) \leq P_{LDis}^{AC} \\ P_{BESS}^{DC}(t) = P_{maxDis}^{DC} \end{cases} \quad \text{or} \quad \begin{cases} P_{BESS}^{AC}(t) = P_{maxDis}^{AC} \\ P_{BESS}^{DC}(t) \leq P_{LDis}^{DC} \end{cases} \quad (3)$$

where P_{maxDis}^{AC} and P_{maxDis}^{DC} are the maximum discharge power of AC and DC BESSs, respectively.

4. Red-Red Regions:

The term ‘‘Red-Red Regions’’ refers to a specific operating condition in the HMG where both the ACMG and the DCMG experience a high-power demand that exceeds the capacity of their respective BESSs. As a result, the BESSs are forced to discharge power beyond their discharging power limit to meet the load demand. This situation can occur when there is a simultaneous surge in power demand from both subgrids or when the available renewable energy generation is insufficient to meet the collective load demand. In such scenarios, the BESSs are subjected to high-stress levels, operating at their maximum discharge capacity, and may face challenges in maintaining voltage and frequency stability. Although both sub-grid BESSs operate at a lower rate than their maximum discharge power rate, the HMG is prone to instability because subgrids cannot support each other. This condition is not a control system weakness, but it should be considered as a system constraint at the design and sizing stage in order to have a broader range of operation. Therefore, the ILC should not exchange power to exacerbate the situation. The below equation denotes this severe scenario.

$$\begin{cases} P_{BESS}^{AC}(t) > P_{LDis}^{AC} \\ P_{BESS}^{DC}(t) > P_{LDis}^{DC} \end{cases} \quad (4)$$

5. Maximum-Maximum Discharge Rate:

Both ACMG and DCMG BESSs operate at their maximum discharge power rate in this scenario. This is the most severe condition of the HMG, and the ILC cannot compensate for the power deficit. The chance of system collapse is very high. Inappropriate sizing of the batteries or other generation units and severe contingency may be the reasons for this scenario. Thus, the ILC should not transfer power between subsystems. This worst case scenario is described as:

$$\begin{cases} P_{BESS}^{AC}(t) = P_{maxDis}^{AC} \\ P_{BESS}^{DC}(t) = P_{maxDis}^{DC} \end{cases} \quad (5)$$

6. Red Region-Maximum Discharge Rate: In the last scenario, one of the BESSs is in the red region, and its counter part is discharging at the maximum rate. Whilst the severity of the contingency is less than case 5, the ILC should not exchange power. This is also a limitation of the system at the design and planning stage. This scenario can be formulated as below

$$\begin{cases} P_{BESS}^{AC}(t) > P_{LDis}^{AC} \\ P_{BESS}^{DC}(t) = P_{maxDis}^{DC} \end{cases} \quad or \quad \begin{cases} P_{BESS}^{AC}(t) = P_{maxDis}^{AC} \\ P_{BESS}^{DC}(t) > P_{LDis}^{DC} \end{cases} \quad (6)$$

The block diagram of the proposed control strategy is represented in Fig. 2.3. The control block can be divided into conventional and adaptive control subsystems. The adaptive control loop includes adaptive per-unit (pu.) and state estimation loops for calculating the value of the adaptive factor based on the characteristics of the BESSs

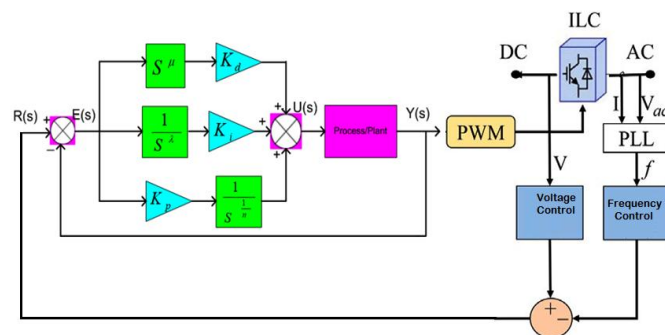


Fig. 2.3 The block diagram of the proposed control strategy

the control strategy to calculate the ILC active power reference maintains the voltage and frequency of the sub grid operating in the steady-state condition. The steady-state condition means insignificant changes in voltage and frequency when the HMG encounters slight variations in its generation or load levels. Nevertheless, this control system cannot regulate the frequency and voltage within their permissible ranges in contingency and heavy load conditions. In this paper, this control strategy is considered as the conventional or Flow tuning interlinking control method [18], and its performance in different study scenarios is demonstrated in the simulations and results section. In order to overcome the shortcoming above, whilst also reducing the stress level on the ILC, a new control approach that adaptively calculates the reference active power for the ILC is proposed. By measuring the instantaneous power of the BESS and comparing it with its maximum rating, the utilization factor, α) for each sub grid is calculated in (7) and (8).

$$\alpha_{DC}(t) = \frac{P_{LDis}^{DC} - P_{BESS}^{DC}(t)}{Max(P_{maxDis}^{DC}, P_{maxDis}^{AC})} \quad (7)$$

$$\alpha_{AC}(t) = \frac{P_{LDis}^{AC} - P_{BESS}^{AC}(t)}{Max(P_{maxDis}^{DC}, P_{maxDis}^{AC})} \quad (8)$$

$$\forall t \quad -1 < \alpha_{DC}(t), \alpha_{AC}(t) < 1$$

Where P_L^D is the discharge rate threshold for the independent operation of each sub-grid and reduces the stress level on the ILC and the BESSs. $P_{AC_{max}^{Dis}}$ and $P_{DC_{max}^{Dis}}$ are the maximum discharging or charging rates of the AC and DC BESSs. $P_{DC_{BES}(t)}$ and $P_{AC_{BESS}(t)}$ are the instantaneous discharging or charging power of DC and AC BESSs, respectively. $\alpha_D(t)$ and $\alpha_{AC}(t)$ represent the normalised values of the available power of DC and AC BESSs which can participate in the adaptive power sharing control loop. Utilising normalised values offers a more comprehensive understanding of the battery's status and conditions, as the nominal capacities and specifications, such as charging and discharging power, can vary between the AC and DC sides' BESS.

When the discharge rate is below P_L^{Dis} , each microgrid can meet its load without relying on power imports from other sub-systems, thus reducing the stress on the ILC by minimizing the power exchange rate. However, if the discharge rate exceeds this threshold, the ILC needs to exchange power adaptively to compensate for power deficits in heavy load conditions. The determination of this threshold depends on several criteria, including the required demand for critical loads, such as hospitals, and the penetration rate of the BESS to maintain system stability and regulation. If the utilisation factor, (t) , is positive, it shows that the sub-grid is operating in the normal condition and can export power to the other subgrid. In contrast, when the utilisation factor is negative, it indicates that the sub-grid is operating in a heavy load condition, or a contingency has occurred, and therefore, the subsystem needs to import power (provided that the other side has surplus power) to regulate the voltage or frequency of the system depending on which sub-grid is facing power deficit. In addition to the discharging/ charging power rate of the BESSs, the proposed control strategy considers the SoC of batteries. The SoC denotes the rate of the remaining energy of the battery at a specific time over the maximum energy of the battery [43]. Hence, an adaptive coefficient, (t) , regarding the SoC is considered in this study. If the SoC level of the BESS is less than the predefined minimum value of that, the BESS cannot support the other sub-grid, as discharging the BESS further below the threshold reduces its lifespan. Similarly, if the SoC level exceeds the maximum predefined limit, the upper limit for the discharge power is set to the maximum nominal discharge power rating. Otherwise, the discharge power is limited to the SoC level according to (9).

$$\gamma(t) = \begin{cases} \gamma_{min} & SoC(t) < SoC_{min} \\ \frac{\gamma_{max} - \gamma_{min}}{SoC_{max} - SoC_{min}} (SoC(t) - SoC_{min}) + \gamma_{min} & SoC_{min} \leq SoC(t) \leq SoC_{max} \\ \gamma_{max} & SoC(t) > SoC_{max} \end{cases} \quad (9)$$

where SoC_{min} and SoC_{max} are the minimum and maximum levels of the SoC. These values should be determined based on the type of battery. γ_{min} and γ_{max} represent the minimum and maximum coefficients regarding the SoC level impact on the proposed adaptive control strategy. The normalised value of exchanging power and its direction is determined in (10). If the power is imported from the AC to the DC side, its sign is negative, and it is positive when transferring power from the DC to the AC subgrid.

$$\beta(t) = Sign(\alpha_{DC}(t) - \alpha_{AC}(t)) \times Min(|\alpha_{DC}(t) \cdot \gamma_{DC}(t)|, |\alpha_{AC}(t) \cdot \gamma_{AC}(t)|) \quad (10)$$

It is clear that the maximum transferable power is limited to the nominal power of the ILC, according to (11).

$$\begin{aligned} & Min(|\alpha_{DC}(t) \cdot \gamma_{DC}(t)|, |\alpha_{AC}(t) \cdot \gamma_{AC}(t)|) - 1 \\ & \leq \beta(t) \leq 1 - Min(|\alpha_{DC}(t) \cdot \gamma_{DC}(t)|, |\alpha_{AC}(t) \cdot \gamma_{AC}(t)|) \end{aligned} \quad (11)$$

The positive value for (t) shows the direction of adaptive power sharing from the DC sub-grid to the AC sub-grid. In contrast, the negative value denotes the direction of adaptive power exchange from the AC microgrid to the DC microgrid. The direction of power sharing in the adaptive control loop complies with the conventional control loop power exchange direction and is constrained within the normalised value corresponding to the nominal capacity of the interlink converter. The value of the adaptive exchanged power is defined in (12).

$$P_{Adp}(t) = \begin{cases} \beta(t) \times P_{maxDis}^{AC} & Sign(\beta(t)) < 0 \\ \beta(t) \times P_{maxDis}^{DC} & Sign(\beta(t)) > 0 \end{cases} \quad (12)$$

P_{maxDis}^{AC} , P_{maxDis}^{DC} are the maximum discharging rate of the AC and DC side BESSs.

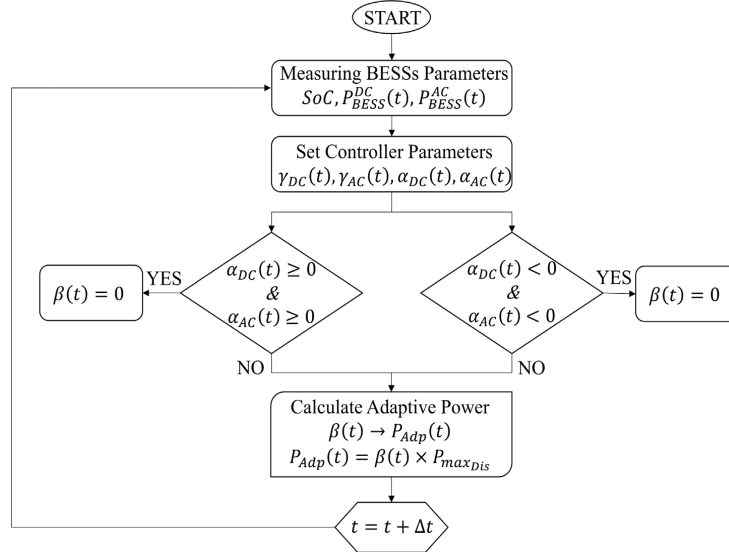


Fig. 2.4 Proposed control strategy conceptual flowchart.

the reference power of the ILC is obtained as expressed in (13)

$$P^* Ref(t) = PRe(t) + PAdp(t) \quad (13)$$

The exchanged power between subsystems based on the conventional control loop is denoted as $PRe(t)$, while $PAdp(t)$ represents the contribution of the adaptive power-sharing scheme in the overall control strategy. These parameters play a crucial role in regulating voltage and frequency and reducing the stress level on BESSs. It is important to note that the adaptive control loop does not transfer power when both sides operate under normal conditions or are in their red zone. The value of this new reference is limited to the nominal capacity of the ILC. In other words, the capacity of the ILC constrains the transferable power between sub-grids.

The conceptual framework of the proposed control strategy is illustrated in Fig. 2.4. The switching frequency of the ILC is 10 kHz. Therefore, the sampling time is ($\Delta t \geq 1 f_{sw} = 10$ ms). The proposed adaptive control strategy is implemented in a decentralized manner, with one individual BESS connected to the point of common coupling of each subsystem. Additionally, the ILC is connected between the point of common coupling of the AC and DC microgrids. This allows the control systems of the ILC and BESSs to interact in a decentralized approach. The proposed control strategy relies on BESSs located near the PCC for their characteristics, including SoC level and instantaneous power. However, a low bandwidth communication link is required between the BESSs on both sides and the interlink converter to facilitate the coordination of the required power exchange. This communication is specifically utilised to transmit data related to the SOC and instantaneous power of the BESSs.

2. Stress intensity index:

To evaluate the performance of the proposed control strategy and quantify the reduction of stress level on the BESS, the stress intensity index is proposed in (20) and takes into account the discharge rate and life cycle loss of the BESS [44]. By measuring this index, the effectiveness of the proposed control strategy can be assessed in reducing stress on the BESS.

This is important because excessive stress can shorten the lifespan of the BESS and reduce its overall performance.

$$SII_{avg} = \frac{1}{T} \int_0^T \frac{SoC_{max}}{SoC(t)} e^{\frac{P_{Dis}(t)}{P_{maxDis}}} dt \quad (14)$$

where SII_{avg} stands for average stress intensity index and T is the total study period. This index shows that the stress level has a reverse relationship with the SoC level, whilst a high discharge power rate exacerbates the intensity of stress level on the BESS. The lower SII_{avg} represents a lower stress level on the BESS.

3. Stability control:

Small signal stability analysis is crucial for evaluating the stability of the proposed control system. The eigenvalue method is used for this analysis. In this method, the state space model of the system is derived and linearized at the operating point, and system stability is evaluated by looking at the system roots locus [45,46]. The influence of the adaptive coefficient on the stability of the proposed control strategy is analyzed using (15).

$$K_{STB} = |(t)| \quad (15)$$

K_{STB} represents stability gain, changing between 0 and 1.

$K_{STB} = 1$ represents the maximum capacity of the ILC.

The droop control and the proposed control loops are considered for stability analysis, The response time of inner voltage and current control loops are quick, and their influences on the stability analysis are not dominant. Therefore their impacts on stability analysis are not considered, and this simplification does not affect the accuracy of analysis [47,48]. For this reason, the aggregated droop coefficients for ACMG sources and DCMG sources are defined in (16) and (17) to represent each sub-grid as a single generation unit.

$$k_p^{AC} = 1 / \left(\sum_{i=1}^n \frac{1}{k_{p_i}^{AC}} \right) \quad (16)$$

$$k_p^{DC} = 1 / \left(\sum_{j=1}^m \frac{1}{k_{p_j}^{DC}} \right) \quad (17)$$

where i and n denote the i th generation unit and their total number on the AC sub-grid, respectively. Similarly, j and m indicate the j th generation unit and their total number on the DC sub-grid, respectively.

Since low-frequency filters affect the performance of the outer droop control layers, their effects are noted in the stability analysis [49]. AC frequency, the DC voltage, and the ILC active power as a result of small signal perturbations can be Model Led as in Eqs. (18), (19), and (20):

$$\Delta f = -k_p^{AC} \frac{\omega_c}{s + \omega_c} (\Delta P_{Load}^{AC} - \Delta P_{ILC}) \quad (18)$$

$$\Delta V = -k_p^{DC} \frac{\omega_c}{s + \omega_c} (\Delta P_{Load}^{DC} + \Delta P_{ILC}) \quad (19)$$

$$\Delta P_{ILC}^* = \frac{\omega_c}{s + \omega_c} ((\Delta V - \Delta f) + K_{STB} \Delta P_{ILC}^*) \quad (20)$$

Where ω_c is the cut-off frequency of filters and Δ stands for the corresponding variable deviation. The small signal equations that are obtained from the (18)–(20) can be formulated as below

$$\Delta \dot{f} = -\omega_c \Delta f + k_p^{AC} \omega_c \Delta P_{ILC} - k_p^{AC} \omega_c \Delta P_{Load}^{AC} \quad (21)$$

$$\Delta \dot{V} = -\omega_c \Delta V - k_p^{DC} \omega_c \Delta P_{ILC} - k_p^{DC} \omega_c \Delta P_{Load}^{DC} \quad (22)$$

$$\Delta \dot{P}_{ILC}^* = \omega_c (K_{STB} - 1) \Delta P_{ILC}^* + \omega_c \Delta V - \omega_c \Delta f \quad (23)$$

Finally, the state space equation for evaluating the stability of the system can be obtained as follow.

$$\dot{X} = AX + BU \quad (24)$$

$$\begin{bmatrix} \Delta f \\ \Delta V \\ \Delta \dot{P}_{ILC}^* \end{bmatrix} = \begin{bmatrix} -\omega_c & 0 & k_p^{AC} \omega_c \\ 0 & -\omega_c & -k_p^{DC} \omega_c \\ -\omega_c & \omega_c & \omega_c (K_{STB} - 1) \end{bmatrix} \begin{bmatrix} \Delta f \\ \Delta V \\ \Delta P_{ILC}^* \end{bmatrix} + \begin{bmatrix} -k_p^{AC} \omega_c & 0 \\ 0 & -k_p^{DC} \omega_c \\ 0 & 0 \end{bmatrix} \begin{bmatrix} \Delta P_{Load}^{AC} \\ \Delta P_{Load}^{DC} \end{bmatrix}$$

Table 1
HMG parameters.

Parameter	Value	Unit
f_n (Nominal frequency)	50	Hz
f_{min}	49.7	Hz
f_{max}	50.3	Hz
f_{sw} (Switching frequency)	10	kHz
$V_{ac_{RMS}}$	380	Volt
V_{DC_n} (DC bus voltage)	700	Volt
$V_{DC_{min}}$	0.95	pu.
$V_{DC_{max}}$	1.05	pu.
ω_c	31.4	rad/s
k_p^{AC}	2×10^{-4}	Hz/W
k_p^{DC}	1.2×10^{-4}	V/W
k_q^{AC}	0.85×10^{-4}	V/Var
$P_{L_{Dci}}$	0.7	pu.
SoC_{min}	20	%
SoC_{max}	80	%
SoC_{AC}	70	%
SoC_{DC}	55	%
$P_{max_{Dci}}^{DC}$	56	kW
$P_{max_{Dci}}^{AC}$	65	kW
$P_{n,ILC}$	20	kW

4. CASE STUDIES AND DISCUSSION

4.1. AC/DC HMG modelling and parameters: The single-line diagram of the under-study HMG depicted in Fig. 7 includes a PV system, a BESS, and AC and DC loads on each sub grid.

The HMG parameters are listed in Table 1. The HMG operates in the islanded mode, and the PV systems operate in the maximum power point tracking (MPPT) condition. As described in Section 2, the proposed autonomous control strategy operates on the basis of the AC sub-grid frequency, DC sub-grid voltage, and SoC and instantaneous charging/discharging power of two buffer BESSs. As a result, the system does not have any limitations on expandability. The nominal capacities of the AC and DC batteries are 100 Ah and 80 Ah, respectively. In this paper, the actual data obtained from PV systems and accumulated loads of a building at Griffith University, which are presented in Fig. 8 are used. The main contribution of this paper is adopting an adaptive power-sharing scheme in heavy load conditions to regulate the voltage and frequency of the HMG. To this end, the performance of the proposed control strategy is demonstrated in instances where the system experiences heavy loading.

4.2. Scenarios

In the following scenarios, the performance of the proposed control strategy is compared with existing methods. The Flow tuning method presented in Eq. (12) [18], the Common bus approach [28], and the Nonlinear exponential droop control method [37], which its mathematical expression discussed in Appendix, are three existing approaches that are adopted to evaluate the effectiveness of the proposed method.

4.2.1. Heavy load condition in AC sub-grid

In this scenario, the DC sub-grid operates under the light load condition, while the ACMG experiences a high load condition with maximum BESS discharge power. The initial total load of the DCMG is 4.9 kW. At $t = 1$ s, the 2.5 kW DC load is disconnected, and at $t = 2$ s, it is reconnected. The AC subsystem load is 60 kW, which is halved at $t = 3$ s. The load demand then increases to its previous amount at $t = 5$ s. The simulation results of this scenario are illustrated in Figs. 9 and 10. The existing interlinking control methods only take into account the pu. error value of the AC side frequency and the DC side voltage. However, as shown in Fig. 9, these methods cause the AC side battery to discharge with its maximum capacity to supply the loads, while the DC side BESS remains in charging or idle mode. Consequently, the DC BESS does not adequately contribute to the ACMG power-sharing, resulting in some volatility in the power profile of the AC sub-grid. In this scenario, the stress level on the BESS of the ACMG is high, which could potentially result in system instability. The fluctuations in voltages and frequency are particularly severe when applying the Flow tuning control system, as shown in Fig. 9(i) and Fig. 10. Even though both the Common bus technique [28] and Nonlinear method [37] aim to enhance power-sharing accuracy and voltage and frequency regulation, their performance during the heavy load switching is not satisfactory. However, with the proposed adaptive control strategy, the DC sub-grid BESS can support the ACMG by participating in power-sharing. Fig. 9(a) and Fig. 9(b) demonstrate that the DCMG can reduce the stress level on the AC BESS by decreasing its discharge power rate. The proposed control strategy regulates the voltage and frequency of the system, thus improving its stability as shown in Fig. 10. By applying the proposed control strategy, the ILC does not transfer power when both sub-grids operate in the light load condition. The result of the proposed adaptive control strategy in Fig. 10(c) shows that during the time period between $t = 3$ s and $t = 5$ s, when both subgrids are in light load condition, the ILC does not exchange power between the subsystems, which proves the effectiveness of the proposed control strategy in reducing the stress on the ILC.

4.2.2. Heavy load condition in DC sub-grid

In this case study, it has been assumed the ACMG operates in a light load condition while the DC subsystem is under a high load condition. The load on the DCMG is 73.5 kW. At $t = 1$ s, a load demand reduction of 49 kW occurs, which is reconnected to the system at $t = 2$ s. The total load of the AC subsystem includes a fixed load with a capacity of 20 kW, and a dynamic load of 10 kW is disconnected and reconnected at $t = 3$ s and $t = 5$ s, respectively. The HMG characteristic profiles, including the ACMG voltage and frequency, the DCMG voltage, their loads and generations, and the ILC exchange power, are presented in Figs. 11 and 12. Figs. 11 and 12 demonstrate that the proposed control strategy outperforms the existing strategies in regulating the DCMG voltage. Additionally, the proposed adaptive control strategy results in less voltage fluctuations. By using the proposed adaptive control strategy, the DCMG imports more power from the AC side to compensate for its generation deficit and also reduces the stress level on its BESS while maintaining the stability of the ACMG. The event occurs on the DCMG while the AC side is operating under a light load condition. No fluctuations are observed in the voltage and frequency of the ACMG, indicating that the system is designed properly to reduce the impact of an event on the performance of the other sub-grid. The effectiveness of the proposed control strategy for regulating the voltage of the DCMG is demonstrated in Fig. 12(a). While both the Common bus technique and the Nonlinear method are more effective than the Flow tuning approach in regulating the DC subsystem voltage, it is evident that their performance is inferior to that of the proposed control system. Similar to the previous scenario, in cases where both sub-grids operate in a light load condition (between $t = 1$ s and $t = 2$ s), the ILC does not exchange power. This is an important consideration for the proposed control strategy, as it helps to avoid unnecessary stress on the ILC.

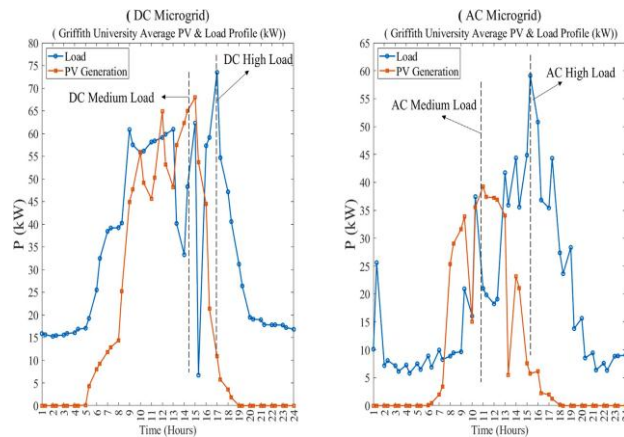


Fig.8. Real data for case study and system modelling.

4.2.3. Medium load condition in AC sub-grid

Two scenarios are considered for evaluating the proposed adaptive control strategy performance in medium load conditions. The objectives of these two scenarios are to lessen the stress level on the BESSs and maintain the reserve capacity for critical loads or sudden load changes. The simulation results for ACMG with medium load, which does not impact the HMG voltages and frequency regulation, are depicted in Fig. 13. The results shown in Fig. 13 indicate that the proposed control strategy performs comparably to the existing methods in terms of voltage and frequency regulation. These findings confirm that the control strategies are well-designed and modelled, and their performances are compared fairly. Fig. 13(f) reveals that power is transferred from the DCMG to the AC sub-grid through the ILC in the medium load condition period of the HMG. This transfer reduces the stress level on the BESS, which is a key objective of the proposed control strategy. Furthermore, the efficiency of Common bus and Nonlinear techniques is better than the Flow tuning approach in mitigating the stress level on the BESS. However, the proposed control algorithm demonstrates superior performance in the reduction of stress level. As long as the load demands do not exceed the BESS maximum discharging capacity, there are no disturbances in the HMG voltage and frequency profiles, regardless of the control method used. Hence, the adaptive control strategy aims to reduce the stress level on the AC side BESS and provide free capacity for potential load increase conditions.

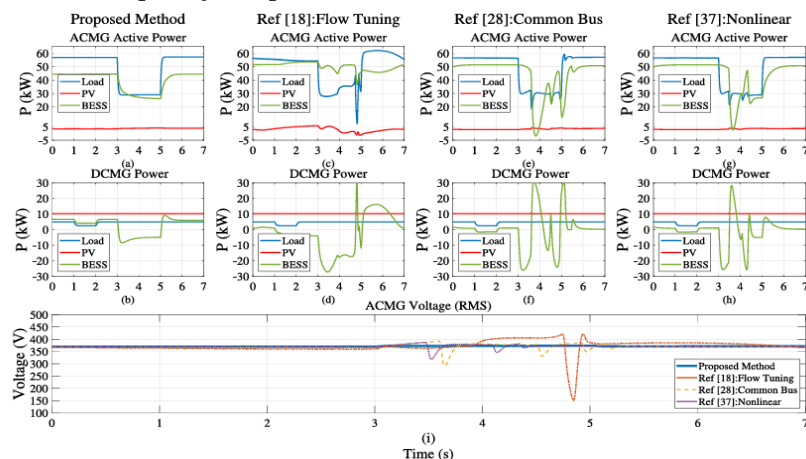


Fig. 9 High load demand in ACMG. (a)–(h): ACMG and DCMG load and generation profiles. (i): Comparing ACMG voltage profiles across different control strategies

4.2.4. Medium load condition in DC sub-grid

This scenario is similar to the previous case study, but in this case, the ACMG is in light load condition, and the DC subsystem supplies the loads within the boundary of its BESS discharge power rate. Fig. 14 represents the results of this study. The results in Fig. 14 are similar to Scenario 3, but according to Fig. 14(f), the direction of exchanged power is reversed, and the ACMG.

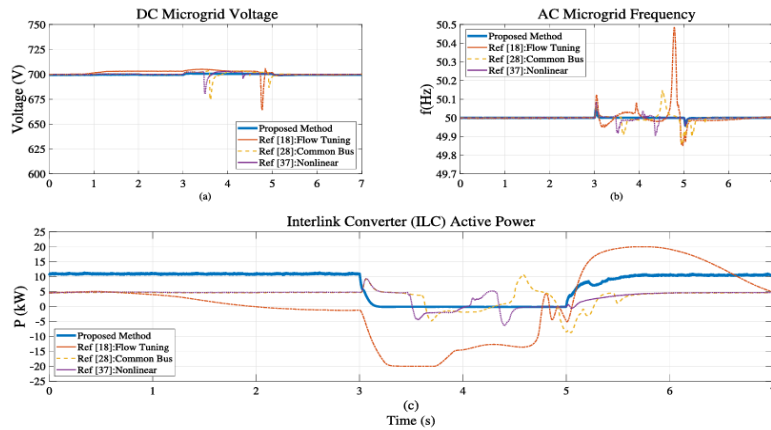


Fig. 10 Comparing the performance of the proposed control strategy with the existing methods.

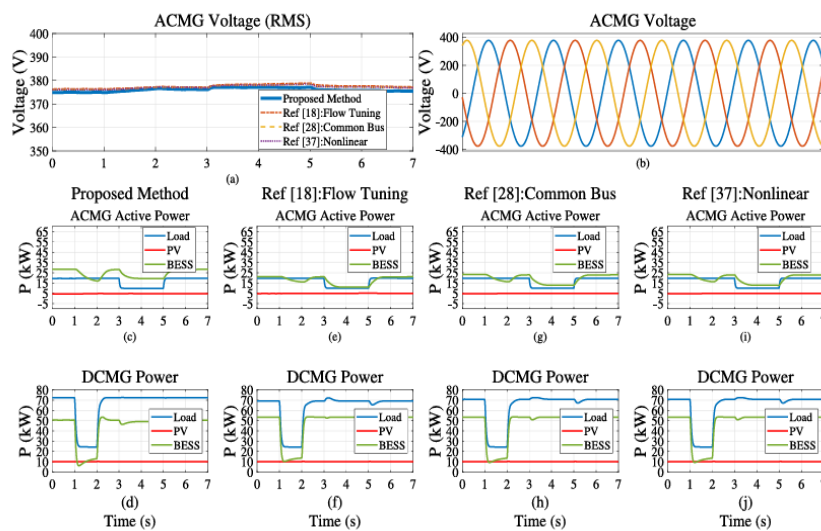


Fig. 11. High load demand in DCMG. (a) and (b): ACMG voltage profile. (c)–(j): ACMG and DCMG load and generation profiles in different control strategies

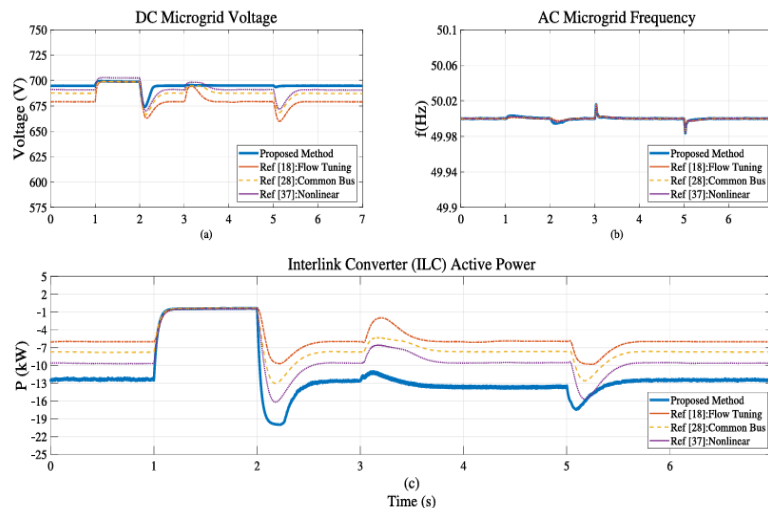


Fig. 12. Comparing the performance of the proposed control strategy with the existing methods.

High load demand in ACMG. (a)–(h): ACMG and DCMG load and generation profiles. (i): Comparing ACMG voltage profiles across different control strategies.

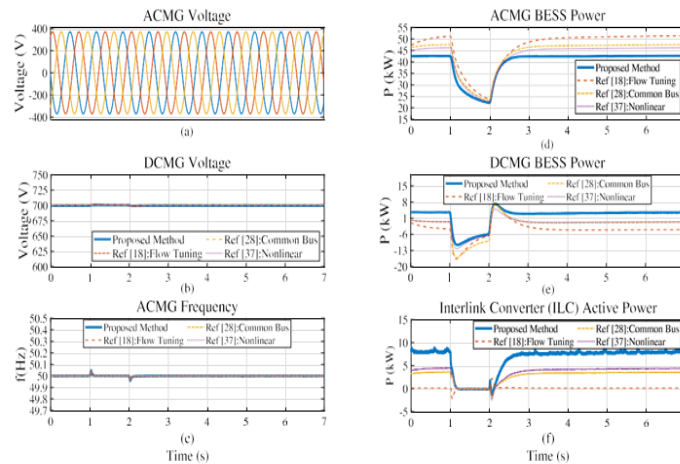


Fig. 13 Performance of the proposed control strategy in ACMG with medium load condition.

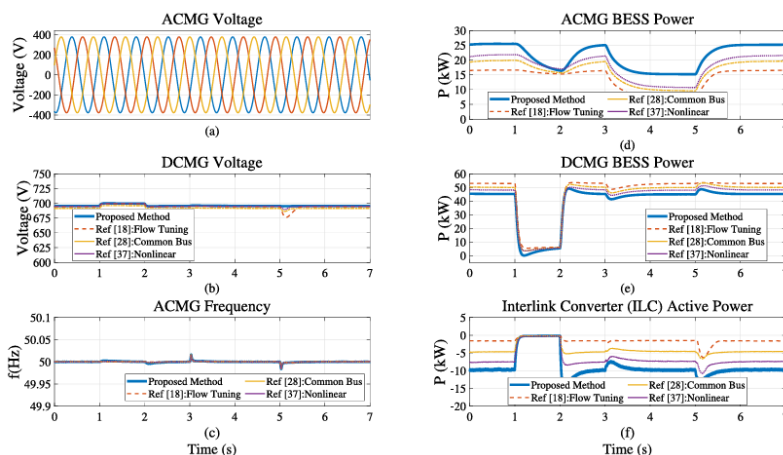


Fig. 14 Performance of the proposed control strategy in DCMG with medium load condition

Table 2 Comparing the stress levels of BESSs in the proposed control strategy with the existing approaches.

Scenario	<i>S/Iavg</i>			Proposed method	<i>Stress relaxation</i> Ref. [18]	<i>compared to:</i>	
	Ref. [18]: Flow tuning	Ref. [28]: Common bus	Ref. [37]: Nonlinear			Ref. [28]	Ref. [37]
1	2.3	2.22	2.12	1.19	12.6%	9.46%	5.19%
2	3	2.86	2.81	2.2	10%	5.59%	3.91%
3	2.22	2.13	2.04	1.4	14.41%	10.8%	6.86%
4	2.95	2.79	2.68	1.45	17%	12.19%	8.6%

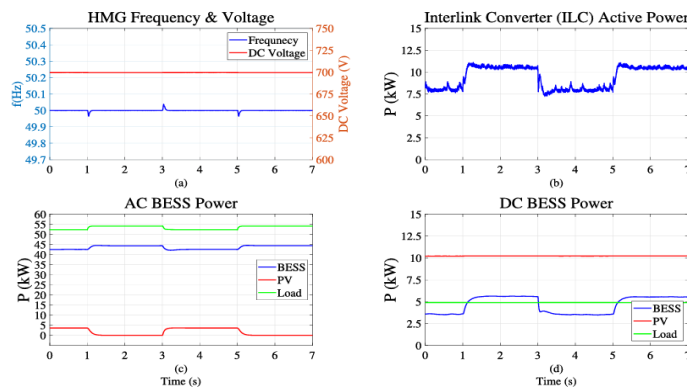


Fig. 15 Plug-and-Play capability evaluation of the proposed control strategy.

Table 3 Comparing MRMSE applying different methods.

Scena rio	X	$MRMSE$			
		Proposed method	Ref. [18]: Flow tuning	Ref. [28]: Common bus	Ref [37]: Nonlin ear
1	f_{AC}	0.010	1.29	0.98	0.74
2	V_{DC}	4.19	21.04	18.47	14.65

4.3. Voltage and frequency control performance evaluation

The Moving Root Mean Square Error (MRMSE) is a derived index from the Root Mean Square Error (RMSE) [50] and is used to compare the performance of the proposed control strategy with the existing approaches in voltage and frequency regulation, as shown in (31). MRMSE is only applied to scenarios 1 and 2, as the performance of both control systems in maintaining voltage and frequency is similar in light and medium load conditions. In scenarios 3 and 4, the focus of the proposed control strategy is to reduce the stress levels on batteries and maintain reserve capacity for critical loads.

$$MRMSE = \sqrt{\frac{1}{\Psi} \int_0^{\Psi} (X_m - X_n)^2} \quad (26)$$

In this equation,
 Ψ is sliding window,
 X , and X_n are measured and nominal values, respectively.

Also, X denotes the AC sub-grid frequency and the DCMG voltage. The control schemes are compared based on the $MRMSE$ index in Table 3. Lower $MRMSE$ values indicate lower system frequency and voltage deviations from their nominal values. By comparing the obtained results, it can be concluded that the proposed approach can significantly reduce HMG frequency and voltage fluctuations in severe operating conditions. In light load and medium load conditions, each subgrid should be capable of operating independently and regulating its voltage and frequency. Therefore, this index is calculated in heavy load conditions.

4.4. Plug-and-play capability Ref.

The proposed control strategy is plug-and-play compliant. To demonstrate this feature, the effects of PV panel shading and retrieval are modelled to analyse the response of the control strategy to a generation source outage and reconnection. To this end, the AC side PV panel is shaded at $t = 1s$, retrieved at $t = 3s$, and then shaded again at $t = 5s$. This sequence of generation unit outage and reconnection may affect the voltage and frequency regulation of the HMG if the control strategy is unable to address it by adjusting the operating point of the ILC. Fig. 15 illustrates that, in the event of shading on the AC side PV system, the ILC transfers additional power from the DC side to the AC sub-grid to offset the power deficit. Furthermore, Fig. 15(a) demonstrates that the control strategy maintains perfect regulation of the voltage and frequency of the HMG during switching instants.

5. CONCLUSION

This paper proposes a new adaptive control strategy for power management in HMG that incorporates BESS characteristics. Simulation results confirm the efficacy of the proposed control strategy in heavy and medium load conditions. Specifically, in heavy load conditions, the proposed control strategy improves system stability by regulating the frequency and voltage of the HMG. In medium load conditions, the stress level on the BESS is reduced through the application of the proposed control strategy, which also keeps a reserve capacity for critical loads or potential load increase scenarios. Furthermore, the proposed control strategy delivers excellent performance in light load conditions, resulting in a reduction in stress levels on the ILC. Additionally, the proposed approach establishes an autonomous control strategy based on the SoC and instantaneous power of the BESSs,

providing the plug-and-play capability to increase the scalability of the proposed control system. The functionality and performance of the proposed control strategy were extensively examined through five case scenarios, employing real PV data. This comprehensive investigation provides insights into the effectiveness of the proposed control strategy.

REFERENCES

1. Guerrero JM, Vasquez JC, Matas J, De Vicuña LG, Castilla M. Hierarchical control of droop-controlled AC and DC microgrids—A general approach toward standardization. *IEEE Trans Ind Electron* 2010;58(1):158–72. <http://dx.doi.org/10.1109/TIE.2010.2066534>.
2. Azeem O, Ali M, Abbas G, Uzair M, Qahmash A, Algarni A, et al. A comprehensive review on integration challenges, optimization techniques and control strategies of hybrid AC/DC Microgrid. *Appl Sci* 2021;11(14):6242. <http://dx.doi.org/10.3390/app11146242>.
3. Torkaman H, Afjei E, Keyhani A, Poursmaeil M. Control and management of hybrid AC/DC microgrid based on $F-Z$ -source converter. *IET Gener Transm Distrib* 2020;14(14):2847–56. <http://dx.doi.org/10.1049/ietgtd.2018.6365>.
4. Pullaguram D, Madani R, Altun T, Davoudi A. Optimal power flow in AC/DC microgrids with enhanced interlinking converter modeling. *IEEE J Emerg Sel Top Ind Electron* 2022. <http://dx.doi.org/10.1109/JESTIE.2022.3145747>.
5. Characteristics of AC/DC hybrid microgrids for precise power sharing. *IEEE Syst J* 2021;15(1):560–9. <http://dx.doi.org/10.1109/JSYST.2020.2984623>.
6. Espina E, Cárdenas-Dobson R, Simpson-Porco JW, Sáez D, Kazerani M. A consensus-based secondary control strategy for hybrid AC/DC microgrids with experimental validation. *IEEE Trans Power Electron* 2020;36(5):5971–84. <http://dx.doi.org/10.1109/TPEL.2020.3031539>.
7. Yang Y, Yang P. A novel strategy for improving power quality of islanded hybrid AC/DC microgrid using parallel-operated interlinking converters. *Int J Electr Power Energy Syst* 2022;138:107961. <http://dx.doi.org/10.1016/j.ijepes.2022.107961>.
8. Wang C, Deng C, Li G. Control strategy of interlinking converter in hybrid microgrid based on line impedance estimation. *Energies* 2022;15(5):1664. <http://dx.doi.org/10.3390/en15051664>.
9. Baharizadeh M, Karshenas HR, Guerrero JM. An improved power control strategy for hybrid AC-DC microgrids. *Int J Electr Power Energy Syst* 2018;95:364–73. <http://dx.doi.org/10.1016/j.ijepes.2017.08.036>.
10. Baharizadeh M, Karshenas HR, Guerrero JM. Control strategy of interlinking converters as the key segment of hybrid AC-DC microgrids. *IET Gener Transm Distrib* 2016;10(7):1671–81. <http://dx.doi.org/10.1049/ietgtd.2015.1014>.
11. Shen X, Shuai Z, Huang W, Chen Y, Shen J. Power management for islanded hybrid AC/DC microgrid with low-bandwidth communication. *IEEE Trans Energy Convers* 2021;36(4):2646–58. <http://dx.doi.org/10.1109/TEC.2021.3073943>.
12. Ahmed M, Meegahapola L, Datta M, Vahidnia A. A novel hybrid AC/DC microgrid architecture with a central energy storage system. *IEEE Trans Power Deliv* 2021;37(3):2060–70. <http://dx.doi.org/10.1109/TPWRD.2021.3103742>.
13. Nabatirad M, Razzaghi R, Bahrani B. Autonomous power balance in hybrid AC/DC microgrids. *Int J Electr Power Energy Syst* 2023;146:108752. <http://dx.doi.org/10.1016/j.ijepes.2022.108752>.
14. Golsorkhi MS, Baharizadeh M. A unidirectional hierarchical control structure with zero power sharing error for hybrid AC/DC microgrid. *IEEE Trans Energy Convers* 2022. <http://dx.doi.org/10.1109/TEC.2022.3207566>.
15. Yang F, Ye L, Muyeen S, Li D, Lin S, Fang C. Power management for hybrid AC/DC microgrid with multimode subgrid based on incremental costs. *Int J Electr Power Energy Syst* 2022;138:107887. <http://dx.doi.org/10.1016/j.ijepes.2021.107887>.
16. Chang J-W, Chae S, Lee G-S. Distributed optimal power sharing strategy in an islanded hybrid AC/DC microgrid to improve efficiency. *IEEE Trans Power Deliv* 2022. <http://dx.doi.org/10.1109/TPWRD.2022.3197434>.
17. Mohamed S, Mokhtar M, Marei MI. An adaptive control of remote hybrid microgrid based on the CMPN algorithm. *Electr Power Syst Res* 2022;213:108793. <http://dx.doi.org/10.1016/j.epsr.2022.108793>.
18. Biglarahmadi M, Ketabi A, Reza Baghaee H, Guerrero JM. Integrated nonlinear hierarchical control and management of hybrid AC/DC microgrids. *IEEE Syst J* 2022;16(1):902–13. <http://dx.doi.org/10.1109/JSYST.2021.3050334>.
19. Li J, Xiong R, Yang Q, Liang F, Zhang M, Yuan W. Design/test of a hybrid energy storage system for primary frequency control using a dynamic droop method in an isolated microgrid power system. *Appl Energy* 2017;201:257–69. <http://dx.doi.org/10.1016/j.apenergy.2016.10.066>.
20. Liu B, Wu T, Liu Z, Liu J. A small-AC-signal injectionbased decentralized secondary frequency control for droop-controlled islanded microgrids. *IEEE Trans Power Electron* 2020;35(11):11634–51. <http://dx.doi.org/10.1109/TPEL.2020.2983878>.
21. Heidari S, Hatami A, Eskandari M. An intelligent capacity management system for interface converter in AC-DC hybrid microgrids. *Appl Energy* 2022; 316:119112. <http://dx.doi.org/10.1016/j.apenergy.2022.119112>.
22. Photovoltaics DG, Storage E. IEEE guide for design, operation, and integration of distributed resource island systems with electric power systems. 2011, <http://dx.doi.org/10.1109/IEEESTD.2011.5960751>.
23. Photovoltaics DG, Storage E. IEEE standard for interconnection and interoperability of distributed energy resources with associated electric power systems interfaces. In: *IEEE std.* 2018, p. 1547–2018. <http://dx.doi.org/10.1109/IEEESTD.2018.8332112>.
24. Abdi H, Mohammadi-ivatloo B, Javadi S, Khodaei AR, Dehnavi E. Energy storage systems. *Distrib Gener Syst* 2017; 7:333–68.

25. Padmanabhan N, Ahmed M, Bhattacharya K. Battery energy storage systems in energy and reserve markets. *IEEE Trans Power Syst* 2019;35(1):215–26. <http://dx.doi.org/10.1109/TPWRS.2019.2936131>.
26. Xu Q. Overview of stability analysis methods in power electronics. In: *Control of power electronic converters and systems*. Elsevier; 2021, p. 169–97. <http://dx.doi.org/10.1016/B978-0-12-819432-4.00018-4>.
27. Eftekharnajad S, Vittal V, Heydt GT, Keel B, Loehr J. Small signal stability assessment of power systems with increased penetration of photovoltaic generation: A case study. *IEEE Trans Sustain Energy* 2013;4(4):960–7. <http://dx.doi.org/10.1109/TSTE.2013.2259602>.
28. Xia Y, Peng Y, Yang P, Yu M, Wei W. Distributed coordination control for multiple bidirectional power converters in a hybrid AC/DC microgrid. *IEEE Trans Power Electron* 2016;32(6):4949–59. <http://dx.doi.org/10.1109/TPEL.2016.2603066>.
29. Chang J-W, Moon S-I, Lee G-S, Hwang P-I. A new local control method of interlinking converters to improve global power sharing in an islanded hybrid AC/DC microgrid. *IEEE Trans Energy Convers* 2020;35(2):1014–25. <http://dx.doi.org/10.1109/TEC.2020.2967416>.
30. Wang J, Jin C, Wang P. A uniform control strategy for the interlinking converter in hierarchical controlled hybrid AC/DC microgrids. *IEEE Trans Ind Electron* 2017;65(8):6188–97. <http://dx.doi.org/10.1109/TIE.2017.2784349>.
31. Yuce E, Minaei S, Tokat S. Root-mean-square measurement of distinct voltage signals. *IEEE Trans Instrum Meas* 2007;56(6):2782–7. <http://dx.doi.org/10.1109/TIM.2007.908153>.
32. Ahmed M, Meegahapola L, Datta M, Vahidnia A. A novel hybrid AC/DC microgrid architecture with a central energy storage system. *IEEE Trans Power Deliv* 2021;37(3):2060–70. <http://dx.doi.org/10.1109/TPWRD.2021.3103742>.
33. Nabatirad M, Razzaghi R, Bahrani B. Autonomous power balance in hybrid AC/DC microgrids. *Int J Electr Power Energy Syst* 2023;146:108752. <http://dx.doi.org/10.1016/j.ijepes.2022.108752>.
34. Golsorkhi MS, Baharizadeh M. A unidirectional hierarchical control structure with zero power sharing error for hybrid AC/DC microgrid. *IEEE Trans Energy Convers* 2022. <http://dx.doi.org/10.1109/TEC.2022.3207566>.
35. Yang F, Ye L, Muyeen S, Li D, Lin S, Fang C. Power management for hybrid AC/DC microgrid with multimode subgrid based on incremental costs. *Int J Electr Power Energy Syst* 2022;138:107887. <http://dx.doi.org/10.1016/j.ijepes.2021.107887>.
36. Chang J-W, Chae S, Lee G-S. Distributed optimal power sharing strategy in an islanded hybrid AC/DC microgrid to improve efficiency. *IEEE Trans Power Deliv* 2022. <http://dx.doi.org/10.1109/TPWRD.2022.3197434>.
37. Mohamed S, Mokhtar M, Marei MI. An adaptive control of remote hybrid microgrid based on the CMPN algorithm. *Electr Power Syst Res* 2022; 213 :108793. <http://dx.doi.org/10.1016/j.epr.2022.108793>.
38. Biglarahmadi M, Ketabi A, Reza Baghaee H, Guerrero JM. Integrated nonlinear hierarchical control and management of hybrid AC/DC microgrids. *IEEE Syst J* 2022; 16(1):902–13. <http://dx.doi.org/10.1109/JSYST.2021.3050334>.
39. Li J, Xiong R, Yang Q, Liang F, Zhang M, Yuan W. Design/test of a hybrid energy storage system for primary frequency control using a dynamic droop method in an isolated microgrid power system. *Appl Energy* 2017; 201: 257–69. <http://dx.doi.org/10.1016/j.apenergy.2016.10.066>.
40. Liu B, Wu T, Liu Z, Liu J. A small-AC-signal injection based decentralized secondary frequency control for droop-controlled islanded microgrids. *IEEE Trans Power Electron* 2020;35(11):11634–51. <http://dx.doi.org/10.1109/TPEL.2020.2983878>.
41. Heidari S, Hatami A, Eskandari M. An intelligent capacity management system for interface converter in AC-DC hybrid microgrids. *Appl Energy* 2022;316:119112. <http://dx.doi.org/10.1016/j.apenergy.2022.119112>.
42. Photovoltaics DG, Storage E. IEEE guide for design, operation, and integration of distributed resource island systems with electric power systems. 2011, <http://dx.doi.org/10.1109/IEEESTD.2011.5960751>.
43. Photovoltaics DG, Storage E. IEEE standard for interconnection and interoperability of distributed energy resources with associated electric power systems interfaces. In: *IEEE std*. 2018, p. 1547–2018. <http://dx.doi.org/10.1109/IEEESTD.2018.8332112>.
44. Abdi H, Mohammadi-ivatloo B, Javadi S, Khodaei AR, Dehnavi E. Energy storage systems. *Distrib Gener Syst* 2017;7:333–68.
45. Padmanabhan N, Ahmed M, Bhattacharya K. Battery energy storage systems in energy and reserve markets. *IEEE Trans Power Syst* 2019;35(1):215–26. <http://dx.doi.org/10.1109/TPWRS.2019.2936131>.
46. Xu Q. Overview of stability analysis methods in power electronics. In: *Control of power electronic converters and systems*. Elsevier; 2021, p. 169–97. <http://dx.doi.org/10.1016/B978-0-12-819432-4.00018-4>.
47. Eftekharnajad S, Vittal V, Heydt GT, Keel B, Loehr J. Small signal stability assessment of power systems with increased penetration of photovoltaic generation: A case study. *IEEE Trans Sustain Energy* 2013;4(4):960–7. <http://dx.doi.org/10.1109/TSTE.2013.2259602>.
48. Xia Y, Peng Y, Yang P, Yu M, Wei W. Distributed coordination control for multiple bidirectional power converters in a hybrid AC/DC microgrid. *IEEE Trans Power Electron* 2016;32(6):4949–59. <http://dx.doi.org/10.1109/TPEL.2016.2603066>.
49. Chang J-W, Moon S-I, Lee G-S, Hwang P-I. A new local control method of interlinking converters to improve global power sharing in an islanded hybrid AC/DC microgrid. *IEEE Trans Energy Convers* 2020; 35(2):1014–25. <http://dx.doi.org/10.1109/TEC.2020.2967416>.
50. Wang J, Jin C, Wang P. A uniform control strategy for the interlinking converter in hierarchical controlled hybrid AC/DC microgrids. *IEEE Trans Ind Electron* 2017; 65(8): 6188–97. <http://dx.doi.org/10.1109/TIE.2017.2784349>.
51. Yuce E, Minaei S, Tokat S. Root-mean-square measurement of distinct voltage signals. *IEEE Trans Instrum Meas* 2007; 56(6): 2782–7. <http://dx.doi.org/10.1109/TIM.2007.908153>.